Contribution from the Department of Chemistry, The University of Chicago, Chicago, Illinois 60637, and Max-Planck-Institut für Festkörperforschung, D-7000 Stuttgart 80, FRG

Molecular Interstitials: An Analysis of the $Gd_2C_2Cl_2$ Structure

Gordon J. Miller,[†] Jeremy K. Burdett,*[†] Christine Schwarz,[‡] and Arndt Simon[‡]

Received April 25, 1986

The recently synthesized compound $Gd_2C_2Cl_2$ contains distinct C_2 dimers occupying the octahedral holes of two adjacent close-packed planes of Gd atoms. By assignment of an effective charge of −4 to C_2, the observed C–C distance is rationalized from the C_2 MO diagram, since the π^* level is half-occupied. In this contribution, we examine the electronic structure and bonding in $Gd_2C_2Cl_2$. Strong Gd–C π bonding is important for giving stability to the structure, while essentially no metal–metal bonding exists at all. The metallic behavior of $Gd_2C_2Cl_2$ is due to the metal–carbon interaction leading to dispersion of the two C_2 π^* bands. We also consider the rotation of the C_2 unit away from the tetragonal axis of the octahedral interstice as in the conceptual transition from CaC_2 to FeS_2 structure type.

Introduction

Isolated M_6X_{12} metal clusters characterize the structures of the metal-rich halides of group 5 transition metals.[1] M_6X_{12} clusters condensed into chains via edge sharing of M_6 octahedra are found with ternary molybdenum oxides, e.g. $NaMo_4O_6$.[2] Strong metal–metal bonds are essential for the stability of these empty clusters. The same type of isolated and condensed M_6X_{12} clusters occur with what were thought to be binary metal-rich halides, MX_n ($n \leq 2.5$) of the group 3 and 4 transition metals M. To our present knowledge all of the M_6X_{12}-type cluster compounds of these metals contain interstitial atoms, e.g. second-row elements: beryllium through oxygen.[3-5] Empty clusters with these metals obviously are not stable due to their electron deficiency arising from a partial occupation of the levels with metal–metal-bonding character. The interstitial atom stabilizes such clusters. In a formal way the carbon atom in, for example, Zr_6CCl_{14}, which is isostructural (except for the C atom) with Mo_6Cl_{14}, adds its four valence electrons to the cluster electrons. Of course, the stabilization of the cluster does not come from the occupation of additional metal–metal-bonding orbitals but primarily from the lowering of those cluster levels that strongly interact with the carbon s and p orbitals.

Most of the interstitial compounds contain single atoms that occupy octahedral or tetrahedral holes between close-packed planes of atoms. Molecular C_2 species frequently occur as interstitials in lanthanoid halides. An interesting class of such halides is the $Gd_2C_2X_2$ structure with X being either Cl or Br.[6,7] The structure contains C_2 units in the octahedral holes between two adjacent close-packed planes of Gd atoms. The dimeric species are specifically oriented parallel to the local pseudo-fourfold axis of the distorted octahedral interstices. This paper examines the bonding and electronic properties of these compounds by using extended Hückel type band calculations.

Structural Observations

The monoclinic layered structure of $Gd_2C_2Cl_2$ contains one Cl–Gd–C_2–Gd–Cl slab per translation along the stacking direction. Figure 1 illustrates a perspective view of the structure onto (010). The single close-packed sheets in the unit cell occupy the positions ABCAB. The midpoint of the C_2 unit falls onto position C. The relative positions of metal and halogen atoms differ from the ZrCl structure[8] where the Cl–Zr–Zr–Cl slab has the sequence ABCA (related to the M_6X_8 cluster). The stacking sequence in $Gd_2C_2Cl_2$ adjusts itself so as to minimize the Coulomb repulsions between the halogen and the interstitial. In addition, the coordination of the metal atoms by the nonmetals is "octahedral" rather than "trigonal prismatic". The specific orientation of the C_2 dimers destroys the trigonal symmetry inherent to a slab Cl–Gd–Gd–Cl with an ABAB sequence. From an isolated octahedral cluster unit Gd_6C_2 of the two-dimensional extended layer, we observe the C_2 unit inclined by only 3° to the pseudotetragonal axis of the elongated octahedron (Figure 2). This orientation essentially corresponds to that of the CaC_2 structure. This particular coordination environment of the C_2 dimer was previously observed in the series of cluster compounds $Gd_{10}C_4Cl_{18}$,[9] $Gd_{10}C_4Cl_{17}$,[9] $Gd_{10}C_4I_{16}$,[10] and $Gd_{12}C_6I_{17}$.[11] The C–C bond distances in these clusters are 1.45 ± 0.02 Å whereas those in the layered materials are 1.27 and 1.36 Å for the bromide and chloride, respectively. Table I contains a listing of some internuclear distances determined

Table I. Internuclear Separations in Compounds Containing Interstitial C_2 Units

compd	*d*(C–C), Å	*d*(M–C), Å	*d*(M–M), Å	ref
$Gd_2C_2Cl_2$	1.36	2.333 (2)	3.95	7
		2.631 (4)	3.62	
		2.671 (4)		
$Gd_2C_2Br_2$	1.27	2.37 (2)	3.45	6
		2.65 (4)	3.832	
		2.66 (4)	3.922	
			4.002	
$Gd_{10}C_4Cl_{18}$	1.47	2.21	3.212	9
		2.51	3.546	
		2.60	3.646	
			3.790	
			4.080	
$Gd_{10}C_4Cl_{17}$	1.47	2.20	3.121	9
		2.49		
		2.58		
CaC_2	1.191	2.595	3.89	13
		2.814	4.21	
LaC_2	1.303	2.635	3.934	13
		2.857	4.305	
TbC_2	1.293	2.462	3.690	13
		2.688	4.058	
LuC_2	1.276	2.344	3.563	13
		2.599	3.904	
UC_2	1.340	2.324	3.517	13
		2.575	3.892	
ThC_2	1.315	2.44 (2)	3.800 (2)	16
		2.66 (2)	3.957 (4)	
		2.78 (2)	4.181 (2)	
		2.90 (2)	4.223 (2)	
		2.94 (2)		
La_2C_3	1.236	2.686 (2)	3.630	17
		2.886 (2)	3.818	
		2.973 (2)	4.019	
ThCN	1.230	2.82 (2)		19
		3.04 (1)		
		3.07 (1)		

(1) Schäfer, H.; Schnering, H. G. *Angew. Chem.* **1964**, *20*, 833.
(2) McCarley, R. E. *ACS Symp. Ser.* **1983**, *No. 211*, 273.
(3) Simon, A. *J. Solid State Chem.* **1985**, *57*, 2.
(4) Ziebarth, R. P.; Corbett, J. D. *J. Am. Chem. Soc.* **1985**, *107*, 4571.
(5) Simon, A. In *Inorg. Solids*; Cheetham, A. K., Day, P., Eds.; Oxford University Press: Oxford, England; in press.
(6) Schwanitz-Schüller, U.; Simon, A. *Z. Naturforsch., B: Anorg. Chem., Org. Chem.* **1985**, *40B*, 710.
(7) Schwarz, C.; Simon, A., unpublished results, 1985.
(8) Adolphson, D. G.; Corbett, J. D. *Inorg. Chem.* **1976**, *15*, 1820.
(9) Warkentin, E.; Masse, R.; Simon, A. *Z. Anorg. Allg. Chem.* **1982**, *491*, 323.
(10) Warkentin, E.; Simon, A., unpublished results.
(11) Simon, A.; Warkentin, E. *Z. Anorg. Allg. Chem.* **1982**, *497*, 79.

[†] The University of Chicago.
[‡] Max-Planck-Institut für Festkörperforschung.

0020-1669/86/1325-4437$01.50/0

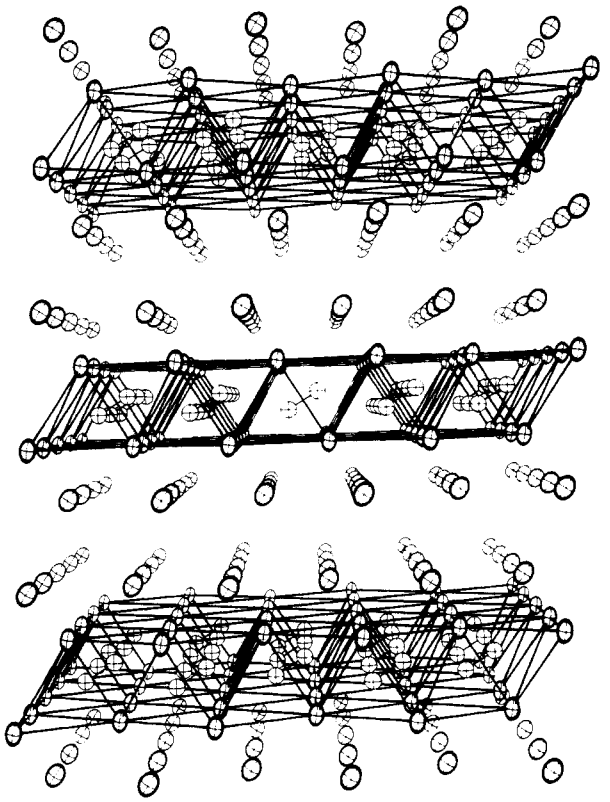

Figure 1. Perspective view of $Gd_2C_2Cl_2$ onto (010). The lines connect Gd atoms in order to emphasize the condensed Gd_6 clusters with interstitial C_2 units.

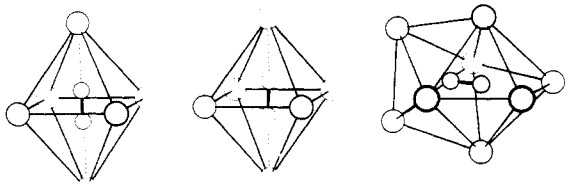

Figure 2. Coordination polyhedra of the C_2 dimers in CaC_2, ThC_2, and La_2C_3.

for the variety of compounds containing interstitial carbon dimers.

Distinct C_2 dimers also exist in metal carbide compounds.[12] In the CaC_2 structure Ca^{2+} and C_2^{2-} ions are arranged as in NaCl, and in the tetragonally distorted low-temperature modification, the C_2 species lie parallel to the tetragonal axis—the C_2 near-neighbor environment is similar in both CaC_2 and $Gd_2C_2Cl_2$. Both alkaline-earth-metal and lanthanoid dicarbides[13] exhibit this structure type as well as some alkaline-earth-metal peroxides[14] and alkali-metal superoxides.[15] Thorium dicarbide is a monoclinic distortion of the CaC_2 structure,[16] in which the orientation of the dimers is no longer along the fourfold direction. Another group of compounds is the lanthanide sesquicarbides, Ln_2C_3, containing a distorted bcc arrangement of metals.[17] The C_2 dimers occupy the holes so that each carbon atom has six nearest-neighbor lanthanoids in an octahedral configuration. The specific orientations of the molecular "anions" maintain cubic symmetry of the unit cell. Figure 2 shows the coordination of C_2 by metals in CaC_2, ThC_2, and La_2C_3. As a final example, a few late-transition-metal

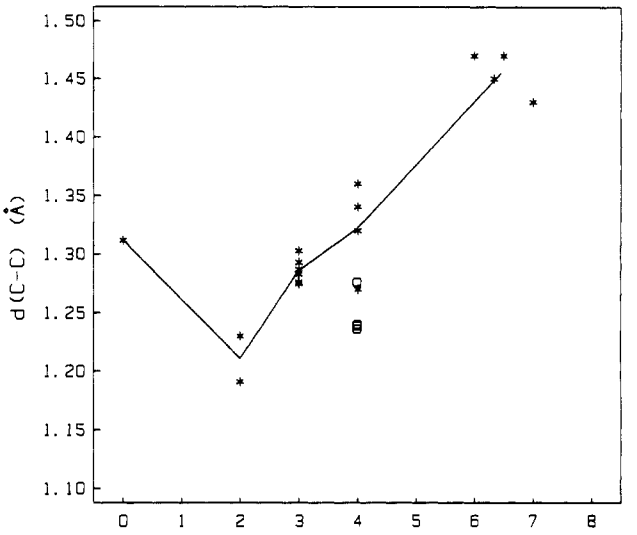

Figure 3. Relationship of the C_2 internuclear distance to its effective negative charge. An asterisk represents C_2 in an octahedral interstice; an open circle represents C_2 in the La_2C_3 structure. The solid line connects the average values of d(C–C) for the asterisk entries.

carbonyl cluster compounds have recently displayed C_2 interstitials.[18]

In all of these systems, except the carbonyl clusters, an ionic treatment in conjunction with the qualitative molecular orbital (MO) scheme for a homoatomic dimer A_2 can be used to reasonably predict the carbon–carbon distance.[3] All anionic species, i.e. nonmetallic elements, in general, are considered closed shell with the resulting negative charge compensated by the appropriate cationic charge. Any valence electrons in excess remain in M–M bonding levels, e.g. in $Gd_{10}C_4I_{16} = (Gd^{3+})_{10}(C_2^{6-})_2(I^-)_{16}(e^-)_2$. For systems with Group 1, 2, or 3 metals or the lanthanoids, we consider them to donate as many of their valence electrons to the nonmetal atoms as these can take. Since the electronegativity of the metals increases from left to right across the periodic table, this treatment becomes less valid with the later transition metals, e.g. FeS_2. Figure 3 illustrates the correlation between the C_2 internuclear distance and the associated effective negative charge. Although there is strictly no complete charge transfer between "anions" and "cations", this electronic assignment to C_2 provides adequate correlation with bond length. When the coordination environment of the dimer changes, however, as in the case for the La_2C_3 structure, the C–C distance is affected, being ~0.05 Å shorter than those observed in CaC_2. So, as the coordination number of the dimer increases, its bond distance decreases. Essentially, we are specifying the electronic configuration of the diatomic species according to the MO scheme **1**. (*Note*: this

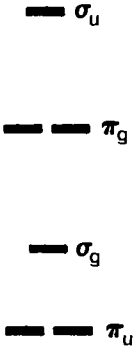

(12) Wells, A. F. *Structural Inorganic Chemistry*, 5th ed., Oxford University Press: London, 1984.
(13) Atoji, M. *J. Chem. Phys.* **1961**, *35*, 1950.
(14) Abrahams, S. C.; Kalnajs, J. *Acta Crystallogr.* **1954**, *7*, 838.
(15) Abrahams, S. C.; Kalnajs, J. *Acta Crystallogr.* **1955**, *8*, 503.
(16) Bowman, A. L.; Krikorian, N. H.; Arnold, G. P.; Wallace, T. C.; nereson, N. G. *Acta Crystallogr., Sect. B: Struct. Crystallogr. Cryst. Chem.* **1968**, *B24*, 1121.
(17) Atoji, M.; Williams, D. E. *J. Chem. Phys.* **1961**, *35*, 1960.
(18) (a) Arrigoni, A.; Ceriotti, A.; Pergola, R. D.; Longoni, G.; Manassero, M.; Masciocchi, N.; Sansoni, M. *Angew. Chem., Int. Ed. Engl.* **1984**, *23*, 322. (b) Albano, V. G.; Chini, P.; Martinengo, S.; Sansoni, M.; Strumolo, D. J. *J. Chem. Soc., Dalton Trans.* **1978**, 459.
(19) Benz, R.; Arnold, G. P.; Zachariasen, W. H. *Acta Crystallogr., Sect. B: Struct. Crystallogr. Cryst. Chem.* **1972**, *B28*, 1724.

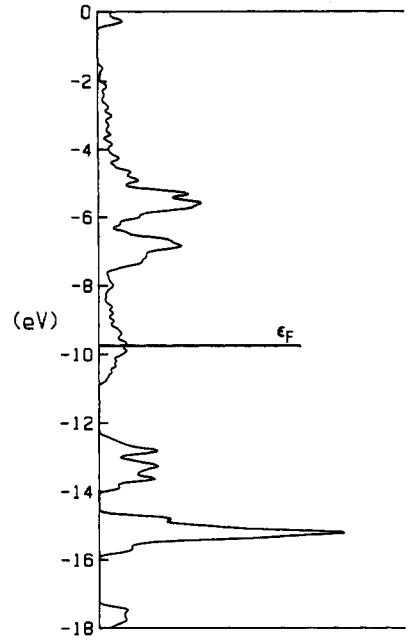

Figure 4. Total density of states of $Gd_2C_2Cl_2$. The Fermi level is marked for 28 electrons per unit cell.

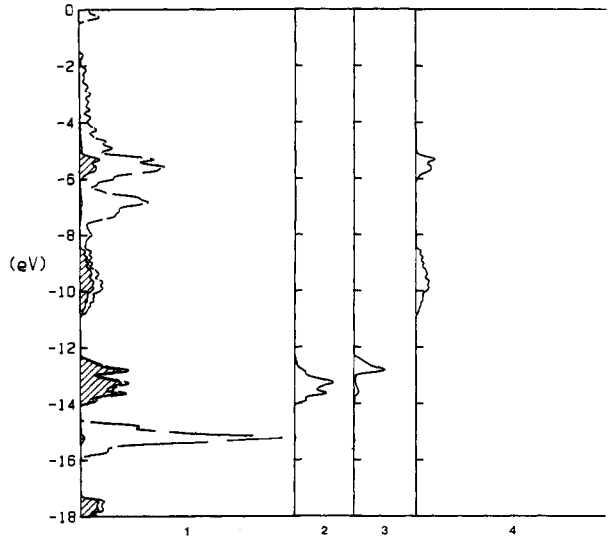

Figure 5. C_2 projections to the total DOS of $Gd_2C_2Cl_2$, proceeding from left to right: (1) total C_2 projection; (2) C_2-π levels; (3) C_2-σ levels; (4) C_2-π^* levels.

diagram ignores the σ_{2s} and σ_{2s}^* levels lying lower in energy.) For 10-electron species, C_2^{2-} as in CaC_2, all σ- and π-bonding levels are completely filled, effecting the shortest bond distance. The 11- and 12-electron systems C_2^{3-} and C_2^{4-} have their π^* levels partially occupied, resulting in increasing separations. This trend continues until all levels contain two electrons, the 18-electron case, for which the diatomic moiety no longer exists.

Electronic Structure of $Gd_2C_2Cl_2$

The previous section noted the effectiveness of the ionic model in predicting the carbon–carbon distance in a variety of compounds containing C_2 units. For $Gd_2C_2Cl_2$ and $Gd_2C_2Br_2$ we may conjecture no metal–metal bonding between Gd atoms since Gd(III) has no electrons available to occupy the appropriate orbitals. Questions concerning the special geometrical arrangement of the C_2 units as well as the cause of the metallic properties, however, remain unanswered. Examination of the orbital interactions in the solid as well as within pertinent fragments provides a more complete analysis. Throughout this paper we will use qualitative molecular orbital methods, in particular extended Hückel theory, which are useful for examining those features controlled by

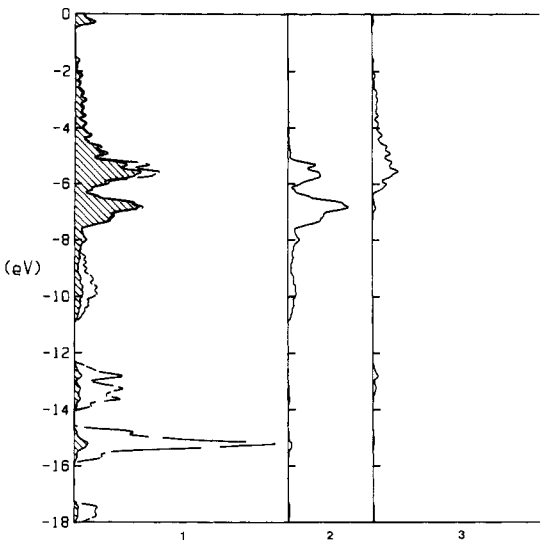

Figure 6. Gd projections of the DOS of $Gd_2C_2Cl_2$, proceeding from left to right: (1) total Gd projection; (2) Gd-"t_{2g}" levels; (3) Gd-"e_g" levels.

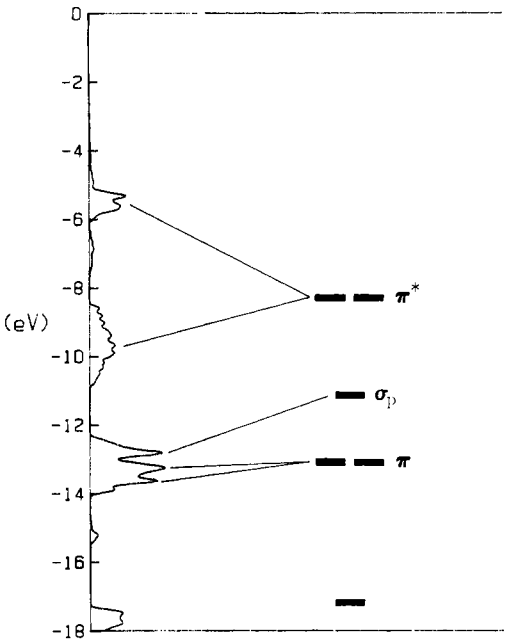

Figure 7. C_2 density of states in $Gd_2C_2Cl_2$ and in the isolated diatomic. d(C–C) is 1.36 Å.

symmetry or angular overlap arguments.[20]

Figure 4 illustrates the total density of states, hereafter abbreviated DOS, for the observed structure of $Gd_2C_2Cl_2$. The DOS is essentially the solid-state equivalent of a molecular orbital energy level diagram. Since $Gd_2C_2Cl_2$ is a layered structure, we performed all calculations in two-dimensional reciprocal space using a centered-rectangular lattice, which has approximately the metric of a trigonal system. A calculation on the complete structure provided similar quantitative results, so using a two-dimensional treatment simplifies the analysis. See the Appendix for further details of the method. To gain an understanding of the electronic nature of the structure, we decompose the total DOS into fragment, atomic, and even individual orbital contributions. Figure 5 shows the C_2 component to the DOS, and Figure 6, the projection of Gd levels. From these two illustrations, we assign the bands as follows: (1) between −16.0 and −14.5 eV lie mostly Cl p levels; (2) from −14.0 to −12.3 eV the three peaks are predominantly the C_2 π and σ_p levels: (3) a strong mixture of C_2 π^* levels (60.0%) and Gd d orbitals (40.0%) occurs from −10.8

(20) Burdett, J. K. *Molecular Shapes*; Wiley: New York, 1980.

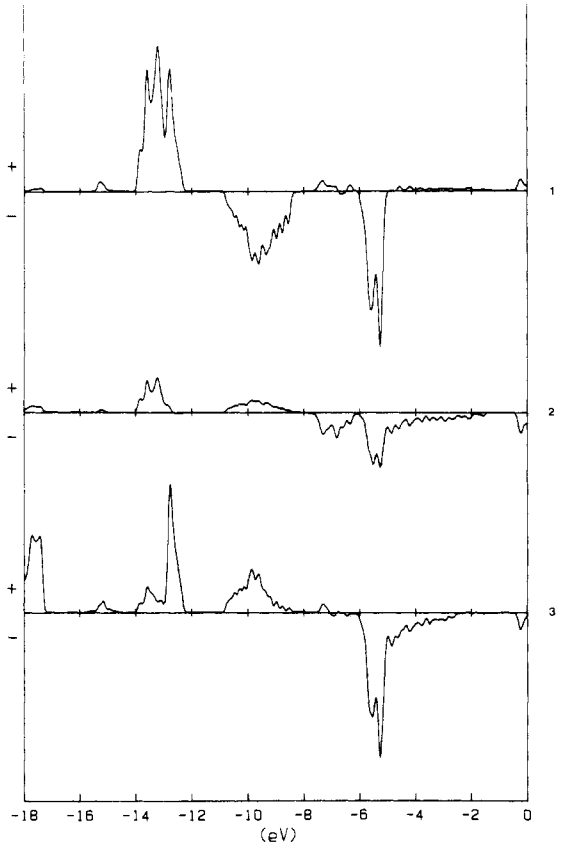

Figure 8. Crystal orbital overlap populations of (1) C-C, (2) Gd_{basal}–C, and (3) Gd_{axial}–C. Both Gd–C COOP curves are scaled by 2.0. +/− indicates bonding/antibonding regions.

to −8.2 eV; finally, (4) the broad metal band extends between −8.2 and −1.5 eV. The separation of the "t_{2g}" and "e_g" bands in the DOS is indicative of the octahedral ligand field around Gd. The Fermi level for 28 electrons per unit cell is −9.73 eV, placing it in the midst of the C_2 π^* bands. This result is consistent with the metallic behavior and the golden appearance of the material.

As with any semiempirical treatment, it is dangerous to make conclusions from the quantitative accuracy of the calculations. Instead, we should examine the orbital interactions based upon overlap and symmetry arguments to interpret the results. With this in mind, what factors control the observed electron count for these materials and what is the principal cause for their metallic behavior? To address the first question, refer to Figure 7, which shows the molecular levels of an isolated C_2 dimer correlated to the C_2 projection to the total DOS of $Gd_2C_2Cl_2$. An examination of the crystal orbital overlap population (COOP) diagrams[21] of C–C and Gd–C interactions (Figure 8) shows that all the occupied metal–carbon bands in the solid have bonding character. Since the interaction energy between two orbitals ϕ_A and ϕ_B is directly related to their overlap integral via S_{AB}^2 as well as inversely dependent in their energy separation, $E_A - E_B \equiv \Delta E_{AB}$,[22] the greatest orbital stabilization occurs for the C_2 π^* level due to Gd–C π-type overlap plus a small ΔE_{AB}. The C_2 σ_p level also shows strong interaction through Gd d_{z^2}–C p_z σ-type overlap. From this preliminary argument, electron occupation proceeds beyond the gap at ca. −12 eV to promote stronger Gd–C bonding. The COOP diagrams further show that the "optimal" electron count reaches a compromise between filling Gd–C bonding and C–C antibonding levels. It would be interesting to attempt oxidizing or reducing $Gd_2C_2Cl_2$, thereby altering the total electron count. If some of the halogen could be replaced by oxygen to form $Gd_2C_2O_xCl_{2-x}$

(21) Applications of COOP curves to metal carbides may be found in: Wijeyesekera, S. D.; Hoffmann, R. *Organometallics* **1984**, *3*, 949.
(22) Albright, T. A.; Burdett, J. K.; Whangbo, M.-H. *Orbital Interactions in Chemistry*; Wiley: New York, 1985.

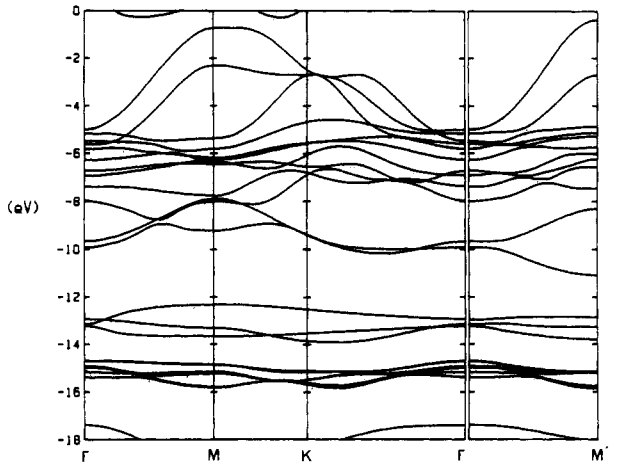

Figure 9. Energy bands for $Gd_2C_2Cl_2$.

without changing the original structure, we would predict a decrease in the C–C distance at the expense of the Gd–C bond strength. Alternatively, intercalating an alkali metal, e.g. Li, between slabs adds electrons to the conduction band, causing the opposite effect. These conclusions utilize a rigid-band model and assume the quaternary atoms to function simply as electron donors or acceptors. No changes in the structure other than bond length variations are taken into account. Possible geometrical alterations as a function of electron count will be considered later in the paper.

The metallic properties of $Gd_2C_2Cl_2$ arise from the dispersion of the two π^* bands. To consider this point, we shall examine the orbital characteristics at various high-symmetry points in the Brillouin zone. The first Brillouin zone, **2**, is based upon a cen-

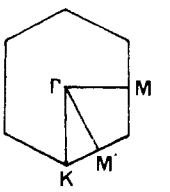

2

tered-rectangular two-dimensional lattice that is nearly trigonal, ergo, the labels of the high-symmetry points. The computed energy bands in the zone are illustrated in Figure 9. The three special directions have the following symmetry properties: (1) ΓM contains a mirror plane perpendicular to the lattice plane; (2) ΓK is parallel to a twofold rotation axis (*Note*: the extension of ΓK intersects M); (3) ΓM′ has no special symmetry properties although extrema in the energy bands occur at M′ because the line is symmorphic and M′ bisects two consecutive Γ points. The three bands of interest are the two C_2 π^* bands (at energies just above −10 eV at Γ) plus a mostly metal-centered band at −8.0 eV at Γ. Representations of these crystal orbitals at Γ are shown in **3**,

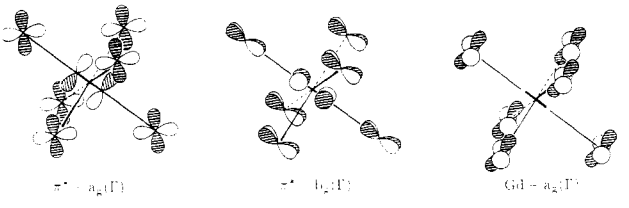

3

which considers only the immediate metal environment around the C_2 π^* orbitals. The symmetry labels are appropriate for the point group C_{2h}, which is isomorphous to the group at Γ.

Considering only Gd–C and Gd–Gd nearest-neighbor interactions, the C_2 π^* bands would be isoenergetic at Γ. However, the reduced symmetry of the system causes a difference in overlap between the two π^* levels on adjacent dimers, slightly favoring the a_g orbital. The metal-centered a_g orbital shows σ bonding among the basal atoms of the octahedral fragment but antibonding

character in the axial–basal direction. What is the nature of the dispersion of these three bands along the different directions in the Brillouin zone (**2**)? The crystal orbital features at any point in the zone are controlled by the phase factor $\exp(i\mathbf{k}\cdot\mathbf{R})$ where $\mathbf{k}$ lies within the zone and $\mathbf{R} = l_1\mathbf{a}_1 + l_2\mathbf{a}_2$. At M the phase factor is $\exp(i\pi l_1)$; +1 for l_1 even and −1 for l_1 odd.

Proceeding along the ΓM direction, all orbitals are classified as either symmetric or antisymmetric with respect to the vertical mirror plane. With reference to **3**, the π^*-a_g and the Gd-a_g orbitals are symmetric while the π^*-b_g orbital is antisymmetric under the reflection operation. (*Note*: the mirror plane is parallel to the plane of the page.) To understand the dispersion of these levels along ΓM, we need to correlate these orbitals at Γ and M according to the reflection operation. Using **3** again, the unit cell we have chosen as the origin contains the two C atoms plus the two axial Gd atoms (the upper left and lower right orbitals of each representation). The basal Gd atoms are all in adjacent unit cells. Since there is no phase change for wave functions in adjacent unit cells at Γ, we clearly see how the orbitals in **3** were constructed. At M, however, the phase factor for these adjacent cells becomes −1, and the resulting crystal orbital representations are shown in **4**.

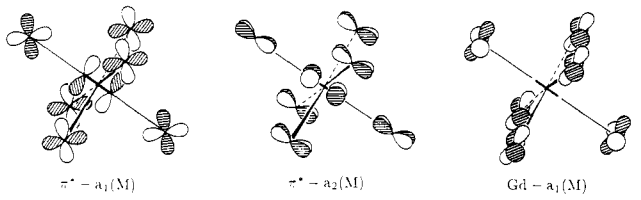

4

Using these two diagrams, we see that along ΓM the π^*-symmetric level becomes destabilized by a π-antibonding interaction between C_2 and the basal Gd atoms while the Gd-symmetric level is stabilized due to axial–basal bonding overlap. Since these two bands are both symmetric, an avoided crossing appears, as shown schematically in **5**. The π^*-antisymmetric orbital energetically

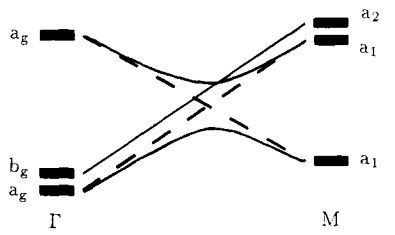

5

rises for the same reasons as its symmetric counterpart but, in this case, can cross the Gd-centered orbital. As diagram **5** shows, if there were no symmetry-mixing, the dispersion of the two π^* bands would be nearly identical. Similar arguments apply to the ΓKM direction though $E(\mathbf{k})$ will have subtle differences. Therefore, the metallic behavior arises from the metal–carbon interactions through similar dispersion characteristics of the two C_2 π^* bands within ~66% of the Brillouin zone.

The Fermi level, however, occurs not at the energetic center of these levels, as one might expect, but rather near the bottom. This location signifies a different dispersion character through other regions of the zone. In a hexagonal cell, ΓM and ΓM′ are related by the sixfold axis, but due to the orientation of the C_2 dimers, the symmetry is reduced, thereby distinguishing these two directions. No special symmetry operations exist along ΓM′ other than the identity, so all bands have the same classification. To qualitatively establish the dispersion relation, we reorient the $Gd_2C_2Cl_2$ layer such that the axial directions of the elongated octahedra are parallel to the z axis. Figure 10 illustrates the correlation of the π^* crystal orbitals between Γ and M′, assuming no mixing. The two bonding Gd–C_2 π^* levels at Γ are split along this direction due to a difference in the π- and δ-type overlap between the C_2 π^* orbital and the appropriate linear combination of basal Gd orbitals. This overlap difference arises via the phase

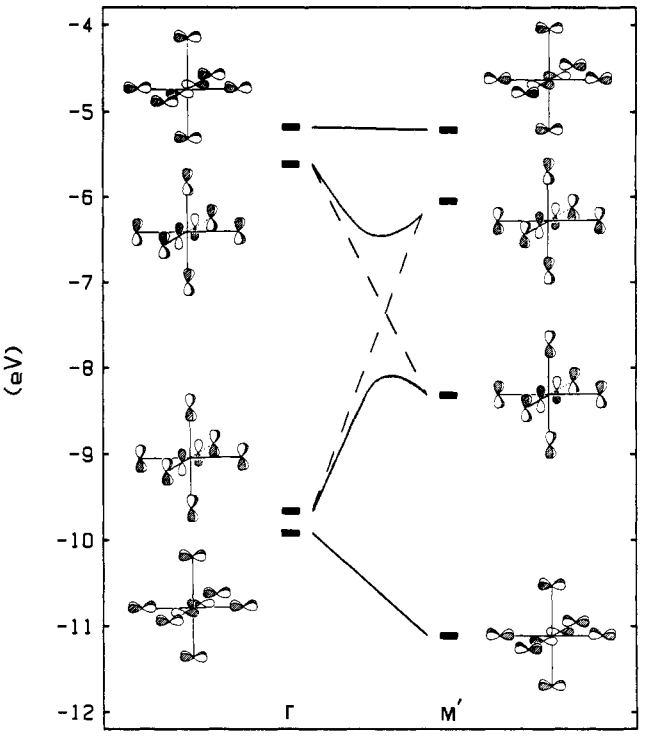

Figure 10. Schematic correlation diagram of the C_2-π^* levels along ΓM′. The splitting at Γ is due to interaction with the axial Gd atoms. The dispersion depends on the phase changes of the basal Gd orbitals.

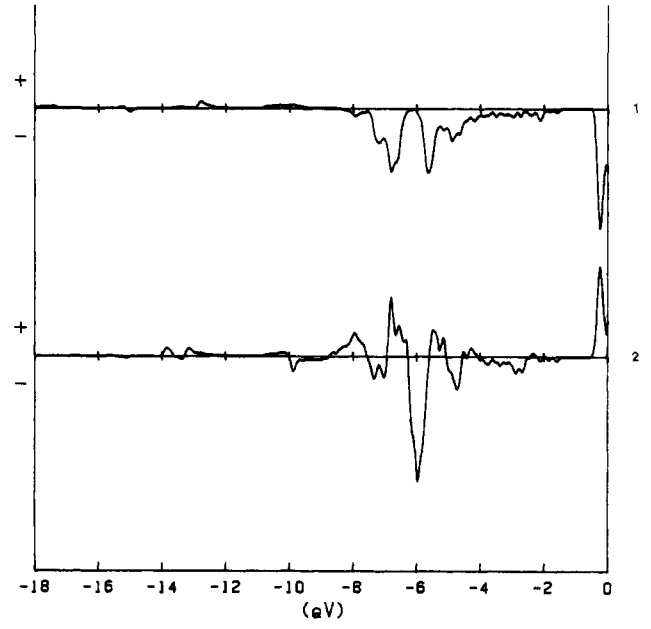

Figure 11. COOP curves of (1) Gd_{basal}–Gd_{axial} and (2) Gd_{basal}–Gd_{basal} interactions. Both curves are scaled by a factor of 2.0. The +/− convention of Figure 8 applies.

factor applied to adjacent unit cell orbitals as previously discussed. This separation accounts for the band width (nearly 2 eV) and the peak shape in the DOS. Furthermore, the lowest band is completely occupied, placing the Fermi energy above its energy maximum. We can now attribute the observed electron count to maximizing the extent of Gd–C_2 π-type bonding.

Metal–Metal Bonding?

Throughout the previous discussion metal–metal bonding never became important. The COOP curves for Gd_{basal}–Gd_{basal} and Gd_{basal}–Gd_{axial} interactions indicate their nonbonding nature; see Figure 11. In the (nonexisting) parent compound GdCl, composed of condensed M_6X_{12} type clusters, Gd–Gd bonding would be essential for stabilizing that structure. However, in $Gd_2C_2Cl_2$ the

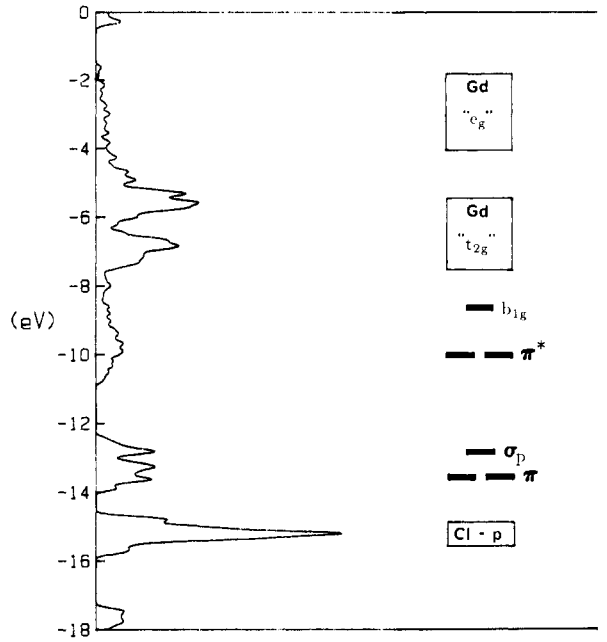

Figure 12. Total DOS of $Gd_2C_2Cl_2$ with a schematic MO diagram for the cluster $Gd_6C_2Cl_{12}^{2+}$. The π, σ, and π^* levels are mostly C_2-centered orbitals; b_{1g} is entirely Gd–Cl centered.

Table II. Charges and Overlap Populations Calculated for $Gd_2C_2Cl_2$ and the $[Gd_2C_2Cl_{12}]^{2+}$ Cluster

	$Gd_2C_2Cl_2$	$[Gd_6C_2Cl_{12}]^{2+}$
q(C)	4.90	4.78
q(Gd)	1.64	1.42 (axial) 1.23 (basal)
p(C–C)	1.25	1.24
$p(Gd_{basal}–C)$	0.13	0.14
$p(Gd_{axial}–C)$	0.50	0.50
$p(Gd_{basal}–Gd_{basal})$	0.02	0.03
$p(Gd_{basal}–Gd_{axial})$	0.01	0.03

dimers inserted between planes of Gd atoms build up strong Gd–C bonds but reduce the interactions between the metal atoms.

We can invoke some Gd–Gd bonding to consider the dispersion in the energy bands near the Fermi level along ΓM′. Certainly, this contributes to some extent to the energetic stabilization of the lower π^* band as seen from the crystal orbital at M′ (see Figure 10). One could measure the effect of metal–metal bonding in this band by setting the overlaps between all Gd atoms to zero. The mechanics of the calculation, however, required these overlaps to be included in order to diagonalize the Hamiltonian matrix.

Cluster Comparisons

As mentioned previously, we can regard $Gd_2C_2Cl_2$ as a condensation of C_2-stuffed Gd_6Cl_{12} clusters. Since the local interactions are qualitatively similar in the isolated cluster and the extended solid, the DOS of $Gd_2C_2Cl_2$ should contain features of the "$Gd_6C_2Cl_{12}$" moiety. Figure 12 indicates the analogy. Although the cluster levels correlate well with the bands in the solid, we gain no insight into their dispersion properties. We do not wish to recapitulate the electronic structure of the M_6X_{12} unit,[23] so Table II lists the pertinent quantitative material derived for the cluster and compares it with analogous quantities of the solid.

Certainly the extended Hückel method, with all its qualitative successes, has suffered with its quantitative reliability. Nevertheless, the computed DOS shows convincing agreement with experimental results, e.g. the measured photoelectron spectrum of $Gd_2C_2Cl_2$ (see Figure 13). Furthermore, our results compare well with the results of more sophisticated theoretical methods.

(23) Bursten, B. E.; Cotton, F. A.; Stanley, G. G. *Isr. J. Chem.* **1980**, *19*, 132.

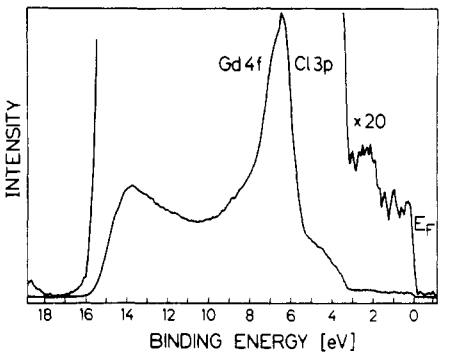

Figure 13. He I (21.2 eV) photoelectron spectrum of $Gd_2C_2Cl_2$.

Table III. Parameters for Extended Hückel Calculations

atom	orbital	H_{ii}, eV	ζ_1 (c_1)[a]	ζ_2 (c_2)[a]
Gd	6s	−7.67	2.14	
	6p	−5.01	2.08	
	5d	−8.21	3.78 (0.7765)	1.381 (0.4587)
C	2s	−21.4	1.625	
	2p	−11.4	1.625	
Cl	3s	−24.2	2.36	
	3p	−15.0	2.04	

[a] Exponents: double-ζ functions are used for transition metals. No f-orbital functions were incorporated for Gd.

Satpathy and Andersen recently reported on the electronic structure of $Gd_{10}C_4Cl_{18}$.[24] They discussed the bonding and structural properties on the basis of a self-consistent density-functional calculation (the LMTO method) and concluded primarily that $Gd_{10}C_4Cl_{18}$ was an ionic compound with no appreciable metal–metal bonding. The observed Gd–Gd distances in the other compounds, $Gd_{10}C_4Cl_{17}$ and $Gd_{12}C_6I_{17}$, were also rationalized by occupation of the LUMO in the cluster calculation—a Gd centered level. Qualitatively, for the Gd parameters shown in Table III, the DOS diagrams for $Gd_2C_2Cl_2$ and $Gd_{10}C_4Cl_{18}$ are similar in the relative positioning of bands, indicating a symmetry-controlled energy scheme and the reliability of extended Hückel theory in such cases.

A Structural Alternative

The most striking geometrical characteristic of $Gd_2C_2Cl_2$ is the orientation of the C_2 dimer with respect to the two adjacent planes of Gd atoms. A rather obvious alternative to the observed structure finds the C_2 dimer parallel to the threefold axis of a ClGdGdCl slab occupying the octahedral holes. This structure type is derived from the observed $Gd_2C_2Cl_2$ configuration by simply rotating the C_2 units within the linear Gd–C–C–Gd fragment. Such a bending distortion can depend upon electron count as observed for the series of molecules: linear C_2F_2 (22 electrons); planar *trans*-N_2F_2 (24 electrons); *skew*-O_2F_2 (26 electrons). A similar sequence is observed for C_2H_2, N_2H_2, and O_2H_2, whose geometries follow from an application of the Nyholm–Gillespie rule.[25] Also, Gimarc has rationalized these geometrical distortions via qualitative MO arguments.[26] By reduction of the point symmetry from $D_{\infty h}$ to C_{2h}, one of the π^* levels is stabilized, favoring the bent configuration for 12- and 14-electron systems. Burdett and McLarnan applied this analysis to the solid-state analogue CaC_2 vs. pyrite, FeS_2, with similar conclusions using only s- and p-orbital functions on the metal.[27] Some anomalies to their electronic results include the alkali-metal

(24) (a) Satpathy, S.; Andersen, O. K. *Inorg. Chem.* **1985**, *24*, 2604. (b) Another recent paper on this topic is: Bullett, D. W. *Inorg. Chem.* **1985**, *24*, 3319.
(25) Gillespie, R. J. *Molecular Geometry*; van Nostrand Reinhold: London, 1972.
(26) Gimarc, B. J. *Molecular Orbital Structure and Bonding: The Qualitative Molecular Orbital Approach*; Academic: New York, 1979.
(27) Burdett, J. K.; McLarnan, T. J. *Inorg. Chem.* **1982**, *21*, 1119.

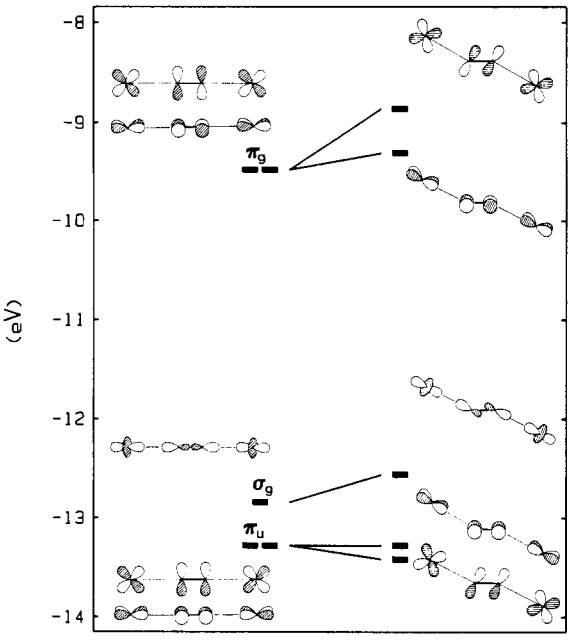

Figure 14. Schematic Walsh diagram for a Gd–C–C–Gd fragment undergoing in-plane bending.

superoxides and alkaline-earth-metal peroxides—14-electron systems with the CaC_2 structure (we note that ZnO_2, CdO_2, and HgO_2 are isostructural with pyrite[12]).

Perhaps a more relevant fragment to examine this distortion would be L_5M-X-X-ML_5 in which the metal d-orbital contributions are included. Tatsumi and Hoffmann, indeed, have already addressed this question in their study of diatom-bridged metalloporphyrin dimers using N_4Fe–O–O–FeN_4 as their prototype.[28] The predictions, however, may be sensitive to the energetic disposition of the metal d orbitals and the π^* levels of the diatomic species. Nevertheless, given that the π^* orbitals of C_2 lie energetically lower than any early-transition-metal levels, we constructed a qualitative Walsh diagram, shown in Figure 14, of Gd–C–C–Gd to examine the bending distortion near a d^0 metal configuration. For a 10-electron system, the σ_g level is the HOMO and the 14-electron system completely occupies the π_g orbitals. Both of the electronic configurations may be effectively assigned as d^0 although there is certainly a large metal component in the π_g levels. From the Walsh diagram, we immediately see that for d^0 10- and 14-electron systems, the local linear geometry is preferred. Like the H_2A_2 case of Gimarc, the σ_g orbital is destabilized on bending due to reduced overlap between a carbon p_z orbital and a Gd d_{z^2} orbital. The C–C σ interaction is reduced as well. More interesting effects occur with the π_g levels. Consider the π^* orbital perpendicular to the plane of the nonlinear fragment. With only nearest-neighbor interactions turned on, the energy of $\pi_{g\perp}$ remains unchanged. However, with all overlaps involved, $\pi_{g\perp}$ is destabilized by the antibonding nature between each Gd and its nonbonded C atom. Furthermore, $\delta_{g\perp}$ mixes with $\pi_{g\perp}$ to a greater extent as the distortion increases, lowering the overlap between nonbonded atoms but also reducing the strength of the Gd–C π bond. Similar effects occur for the $\pi_{g\parallel}$ orbital except that the interactions are stronger, i.e. more σ type than π type, which mix by symmetry. Therefore, we can rationalize the CaC_2 geometry for the d^0 examples from this isolated fragment model. How does this analysis compare with calculations on the $Gd_2C_2Cl_2$ alternative?

Figure 15 compares total energies for the actual structure with the trigonal alternative under a constant unit cell volume as a function of electron count. Though the alternative is energetically favored at every point (only 0.05 eV separate the two at 28 electrons), the trend emphasizes the preference for the observed geometry at 28 electrons. The energy zero can shift by adjusting

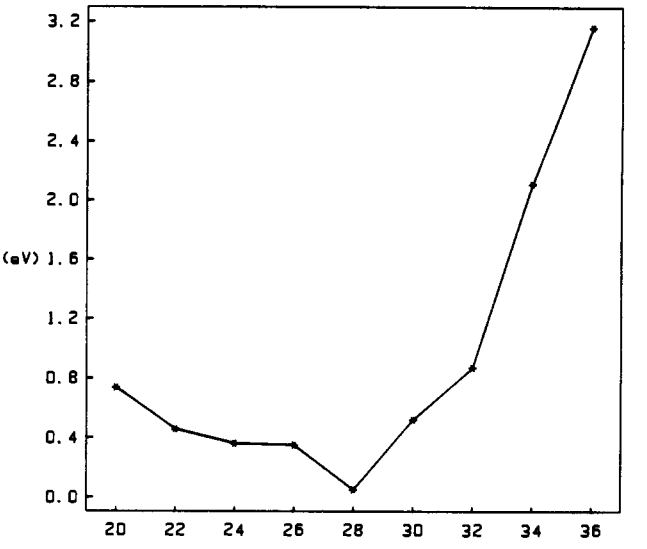

Figure 15. Energy difference between the observed and alternative $Gd_2C_2Cl_2$ structures as a function of electron count. Positive ΔE values indicate the alternative geometry is calculated to be more energetically stable.

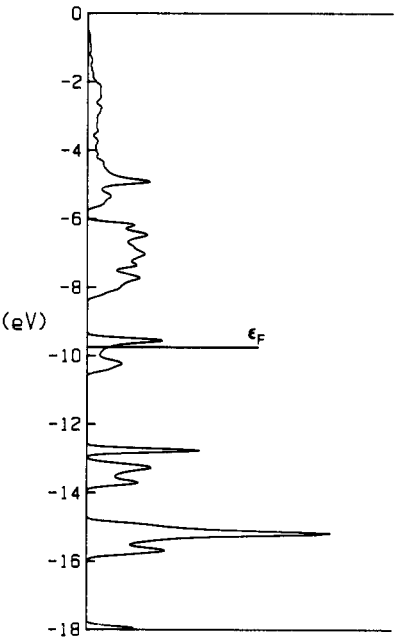

Figure 16. Total DOS of the alternative $Gd_2C_2Cl_2$ structure. The Fermi level for 28 electrons per cell is −9.75 eV ("low-spin" case).

the geometrical parameters, but the overall shape remains unchanged. We note this sensitivity as an outcome of the coordination number problem and emphasize the energetic changes as electrons are added or removed from the bands.

The total DOS for the $Gd_2C_2Cl_2$ alternative structure is illustrated in Figure 16, in which we discover additional energy gaps: the C_2 π^* band splitting away from the Gd levels, as well as the Gd levels themselves separating into two sections. Furthermore, the dispersion of the π^* and σ levels are reduced. Recall that the specific orientation of the C_2 dimers in the octahedral interstices provided strong π-type interactions with both apical and basal metal atoms to account for the wide π^* band. Also, one π^* level was not restricted by symmetry to directly overlap the metal region. As the dimers are gradually tilted, this π overlap between basal Gd and the C_2 unit is removed. Moreover, the crystal orbital features of the π^* bands change considerably along the two high-symmetry directions in the trigonal Brillouin zone, ΓM and ΓK (see Figure 17), suggesting a multitude of avoided crossings occurring between metal-centered and π^*-centered bands. These two effects suffice to produce narrow bands in the alternative

(28) Tatsumi, K.; Hoffmann, R. *J. Am. Chem. Soc.* **1981**, *103*, 3328.

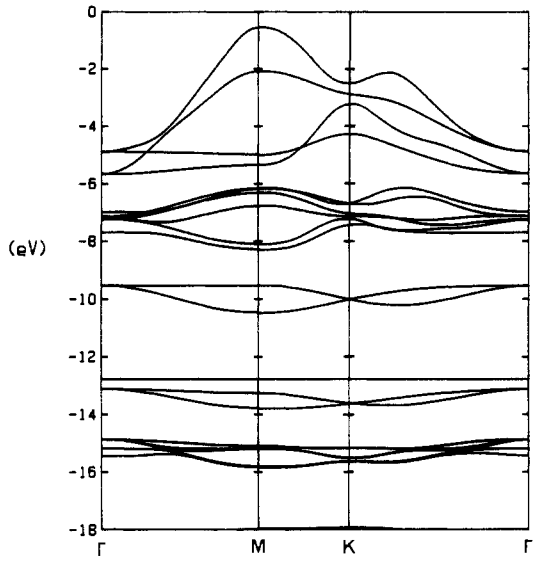

Figure 17. Energy bands for the alternative $Gd_2C_2Cl_2$ structure.

structure. The Fermi level resides in the narrow, but partially filled, π^* band. For narrow band systems, however, electron-electron repulsion may cause each band orbital to be singly occupied by electrons with parallel spin.[29] Therefore, the alternative could show properties consistent with a magnetic semiconductor, but we are unable to predict whether intercell forces would produce a ferromagnetic or an antiferromagnetic ground state.

Returning to the energy difference curve of Figure 15, the predominant dispersion in the π^* band accounts for the minimum. For lower electron counts, the curve compares occupied levels that are essentially localized on the nonmetals. Their relative energies are certainly sensitive to the magnitude of the overlap with Gd orbitals and seemingly favor the trigonal species. The fragment calculation is apparently in conflict with the solid-state results. However, on bending the dimer, we change the coordination of each carbon atom by its Gd neighbors. Nevertheless, in this layered environment with weakened Gd–C bonds, we may expect these dimeric species to become less rigidly held in their observed configuration. Beyond 28 electrons, the dispersion of π^* destabilizes the observed structure with respect to the alternative. Therefore, we may anticipate that alkali-metal intercalation would tend to realign the C_2 dimers with concomitant lengthening of the C–C distance.

(29) Whangbo, M.-H. *J. Chem. Phys.* **1980**, *73*, 3854.

Questions and Conclusions

In this paper we directed attention to the structural chemistry of $Gd_2C_2Cl_2$. We emphasized the importance of π interactions between Gd and C_2 for (1) stabilizing the observed orientation of the dimer in the octahedral holes, (2) setting the electron count at 28 electrons per formula unit, and (3) providing its metallic properties. The ionic model coupled with a qualitative MO scheme of a main-group dimer provided an indicator for the C–C bond length but gave no information about Gd-C bonding. Furthermore, we concluded that metal–metal bonding was not a major factor in these materials but did contribute to auxiliary effects, mostly in the dispersion of the bands near π^*.

The structure and bonding of $Gd_2C_2Cl_2$ raise a number of interesting questions. Are changes of the valence electron concentration possible, e.g. by intercalation reactions or by chemical substitution both in anion and cation sites? Do such changes reflect in the C–C bond length and in the orientation of the C_2 unit, which could serve as an indicator for the valence electron concentration? Are other dimeric interstitial species possible, e.g. CN, BN, and even B_2?

Acknowledgment. G.J.M. wishes to thank The Electrochemical Society for supporting his visit to MPI via the F. M. Becket Memorial award. The research at Chicago was supported by NSF Grants DMR 8414175 and DMR 8216892.

Appendix

All of the calculations described in this paper used the extended Hückel method[30] both for the molecular orbital calculations on the fragments and for the tight-binding computations on the crystalline solids. The atomic parameters are listed in Table III.

The following geometrical constraints were applied: (1) the C–C distance was maintained at 1.36 Å; (2) in the observed $Gd_2C_2Cl_2$ structure, we set $d(Gd_{axial}–C)$ to 2.33 Å, $d(Gd_{basal}–C)$ to 2.65 Å, and d(Gd–Cl) to 2.81 Å. For the alternative structure, the same unit cell volume as for the observed structure was used. All lattice sums included third nearest-neighbor cells in the two directions. For the centered-rectangular cell, 72 special points were used, and for the hexagonal cell, we selected 105 special k-points, both in the irreducible wedges of their respective Brillouin zones.

(30) (a) Hoffmann, R. *J. Chem. Phys.* **1963**, *39*, 1397. (b) Whangbo, M.-H.; Hoffmann, R. *J. Am. Chem. Soc.* **1978**, *100*, 6093. (c) Ammeter, J. H.; Bürgi, H.-B.; Thibeault, J. C.; Hoffmann, R. *J. Am. Chem. Soc.* **1978**, *100*, 3686.

Notes

Contribution from the Central Research and Development Department, Experimental Station 328, E. I. du Pont de Nemours & Company, Wilmington, Delaware 19898

Electrocrystallization of Poorly Conducting Charge-Transfer Complexes

Michael D. Ward

Received May 20, 1986

Electrocrystallization is a convenient technique for the synthesis of conducting and superconducting one-dimensional "organic metals" such as pyrene,[1] tetrathiafulvalene,[2,3] tetramethyltetraselenafulvalene,[4] and recently bis(ethylenedithio)tetrathiafulvalene complexes.[5,6] However, this method has not been exploited for poorly conducting charge-transfer complexes, which are generally prepared by cooling of saturated solutions or by metathetical methods. Precise control of the rate of crystallization,

(1) Chiang, T. C.; Reddoch, A. H.; Williams, D. F. *J. Chem. Phys.* **1971**, *54*, 2051.

(2) Kathirgamanathan, P.; Mucklejohn, S. A.; Rosseinsky, D. R. *J. Chem. Soc., Chem. Commun.* **1979**, 86.

(3) Wheland, R. C.; Gillson, J. L. *J. Am. Chem. Soc.* **1976**, *98*, 3916.

(4) Bechgaard, K.; Jacobsen, C. S.; Mortensen, K.; Pedersen, H. J.; Thorup, N. *Solid State Commun.* **1980**, *33*, 1119.

(5) Williams, J. M.; Carneiro, K. *Adv. Inorg. Chem. Radiochem.* **1985**, *29*, 249.

(6) (a) Parkin, S. S.; Engler, E. M.; Schumaker, R. R.; Lagier, R.; Lee, V. Y.; Scott, J. C.; Greene, R. L. *Phys. Rev. Lett.* **1983**, *50*, 270. (b) Satio, G.; Enoki, T.; Toriumi, T.; Inokuchi, H. *Solid State Commun.* **1982**, *42*, 557. (c) Williams, J. M.; Emge, T. J.; Wang, H. H.; Beno, M. A.; Copps, P. T.; Hall, L. N.; Carlson, K. D.; Crabtree, G. W. *Inorg. Chem.* **1984**, *23*, 2558.

0020-1669/86/1325-4444$01.50/0